Applied Catalysis B: Environmental 244 (2019) 965–973

Contents lists available at ScienceDirect

Applied Catalysis B: Environmental

journal homepage: www.elsevier.com/locate/apcatb

Aerobic oxidation of 5-hydroxymethylfurfural to 2,5-furandicarboxylic acid over Co/Mn-lignin coordination complexes-derived catalysts

Hua Zhou, Huanghui Xu, Yun Liu*

Beijing Key Laboratory of Bioprocess, College of Life Science and Technology, Beijing University of Chemical Technology, Beijing 100029, China

ARTICLE INFO

Keywords:
Heterogeneous catalyst
Aerobic oxidation
2,5-Furandicarboxylic acid
5-Hydroxymethylfurfural
Lignin

ABSTRACT

Deriving more valuable products from renewable lignocellulosic biomass is attractive but still remains major challenges, the insufficient lignin valorization is considered as one of the main obstacles. Here, we report a novel catalyst comprised of cobalt nanoparticles (NPs) encapsulated in graphitic carbon tailored with manganese and nitrogen heteroatoms (Co-Mn/N@C), fabricated by pyrolyzing a mixture of Co/Mn-lignin complex and dicyandiamide. The as-synthesized Co-Mn/N@C catalyst exhibits excellent activity and recyclability for oxidizing biomass-derived 5-hydroxymethylfurfural (HMF) into 2,5-furandicarboxylic acid (FDCA) in aqueous system using O_2 as oxidant. The structure-performance relations of the catalyst are investigated, suggesting that Mn/N-doped carbon can activate the reactivity of Co NPs for HMF oxidation by tuning the electronic structure of embedded metal NPs. Additionally, isotopic labelling experiments reveal the role of water and O_2 for FDCA production using Co-Mn/N@C as catalyst. This work not only demonstrates the integrated biorefinery strategy, but also provides a new approach for sustainable, low-cost heterogenous catalysts preparation.

1. Introduction

Selective oxidation of biomass-derived platform chemicals to renewable commodities or their alternatives has attracted immense scientific interests [1–3]. Among these compounds, 2, 5-furandicarboxylic acid (FDCA) is one of the high value-added renewable chemicals produced from C6 sugars-derived 5-hydromethyl furfural (HMF) [2–5]. The most attractive application of FDCA is used as a substitute of petroleum-based terephthalic acid in the synthesis of polyesters, polyamides, polyurethanes, coating resins and metal-organic frameworks (MOFs) [6–9]. It has been extensively investigated on the catalytic oxidation of HMF to FDCA, especially for heterogeneous catalysts using molecular oxygen (O_2) as low-cost and environmentally friendly oxidant [10–14]. As shown in Scheme 1, supported noble metal catalysts (e.g., Au, Pt, Pd) [5,12,14,15] and non-noble metallic oxides (such as Mn-Fe mixed oxide, Co_3O_4) [11,16] have been developed for the manufacture of FDCA. However, the scarcity and high cost of the noble metals and the inefficient activity of metal oxides impede the industrial scale production of FDCA. Thus, *de novo* design of effective, inexpensive, and non-precious metal-based heterogeneous catalysts for selective HMF oxidation is still challenging and of enormous demands.

Recently, construction of heterojunctions between metallic NPs and tailored carbon is emerging as an effective strategy to activate the reactivity of the embedded metallic NPs [17–19]. In this regard, N-doped carbon supported metal-based catalysts have exhibited outstanding performance in oxygen reduction reaction [20,21], oxidative esterification [22,23], hydrogenation [24,25], environmental remediation [26,27], *etc*. The current strategies for construction of this type of heterogeneous catalysts are commonly explore various MOFs [28–30], metal-ligand molecules deposited on carbon black [31,32], and polymers [33,34] as precursors. Despite these well-established methods, the practical application of these catalysts is still limited by the unsustainability and high-cost of petroleum-based ligands and/or supports (e.g. Vulcan XC72R, PTA, 2-methylimidazole, 1, 10-phenanthroline). Instead, using biomass wastes as precursors for fabricating high-quality carbon materials as catalysts support has significant economic and environmental effects by eliminating agricultural and forestry wastes induced pollution and decreasing the utilization of fossil resource [21,26].

For the objective of biomass valorization, we recently developed a bioinspired assembly process of metal-organic complexes using lignin as macromolecular ligand, the second abundant polymer from lignocellulose. Herein, we report a sustainable approach for synthesizing Mn and N co-doped carbon supported cobalt nanocatalysts (Co-Mn/N@C) using Co/Mn-lignin complexes and dicyandiamide as precursors for aerobic HMF oxidation. The structural properties of the resulting

* Corresponding author.
E-mail addresses: liuyun@mail.buct.edu.cn, liuyunprivate@sina.com (Y. Liu).

https://doi.org/10.1016/j.apcatb.2018.12.046
Received 18 September 2018; Received in revised form 9 December 2018; Accepted 17 December 2018
Available online 17 December 2018
0926-3373/

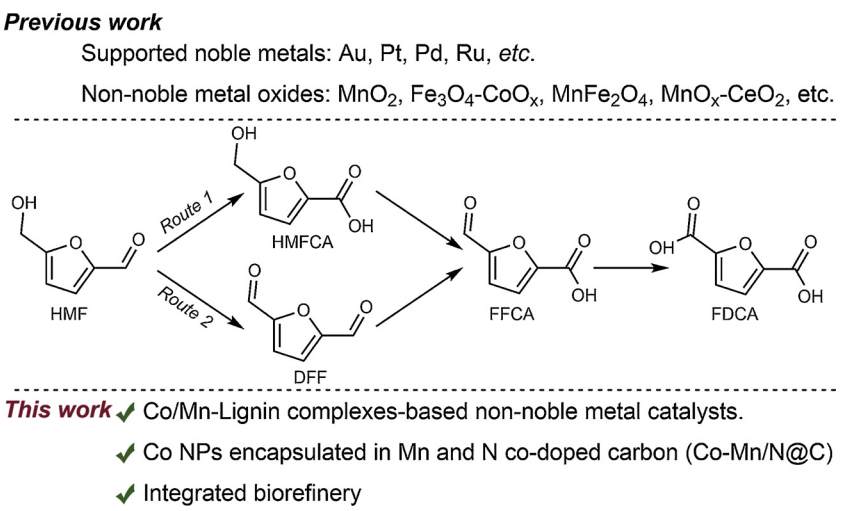

Scheme 1. Heterogeneous catalysts for aerobic oxidation of HMF to FDCA.

catalysts are characterized by TEM, EDX, XRD, XPS, CO_2-TPD, H_2-TPR, and Raman spectroscopy. Furthermore, the effects of Mn and N co-doped carbon on the reactivity of Co NPs are also investigated through kinetic reactions. Additionally, the role of H_2O and O_2 in aerobic HMF oxidation over Co-Mn/N@C catalyst is studied by isotopic labeling experiments using $H_2{}^{18}O$ and $^{18}O_2$. For the first time, we describe the reaction pathway and mechanism for oxidizing HMF to FDCA over Co NPs encapsulated in Mn/N co-doped carbon.

2. Experimental section

2.1. Materials

Alkali lignin (471,003), dicyandiamide (DCA, 99%), 5-hydroxymethylfurfural (≥99%), and 5-formyl-2-furoic acid (FFCA, CPR) were purchased from Sigma-Aldrich. 2,5-Diformylfuran (DFF, 98%) and 2,5-furandicarboxylic acid (98%) were purchased from Suzhou Guide Fine Materials Co., LTD. 5-Hydroxymethyl-2-furancarboxylic acid (HMFCA, 98%) was purchased from Bide Pharmatech LTD. Cobalt nitrate ($Co(NO)_2{\cdot}6H_2O$) and manganese sulfate ($MnSO_4{\cdot}H_2O$) were analytical purity and purchased from Tianjin North Fine Chemicals Development Co., LTD. $H_2{}^{18}O$ (97%) was purchased from Shanghai Aladdin Bio-Chem Technology Co., LTD. $^{18}O_2$ (≥97%) was purchased from Shanghai Research Institute of Chemical Industry. All reagents were used as received without any further purification.

2.2. Synthesis of metal-lignin coordination complexes

Typically, 10 g lignin was dissolved into 1000 mL of deionized water with magnetic stirring in a 2000 mL beaker. Then, metal ions solution (500 mL) containing Co^{2+} (40 mmol) and Mn^{2+} (10 mmol) was added into the lignin solution with robust stirring. The pH of the mixture solution was adjusted to 6.8 with aqueous ammonia (10%); it was kept stirring for 1 h at room temperature. The formed metal-lignin complex was obtained by centrifugation at 5000 rpm for 5 min and rinsed with water for three times, then dried in air at 80 ℃ overnight. The as-prepared metal-lignin complex was denoted as Co_4Mn_1-L. Similarly, other types of metal-lignin complexes were prepared and denoted as Co_xMn_y-L, where x + y = 5. "x" and "y" represent the amount (mmol) of added Co and Mn per gram of lignin, respectively, during the assembly process.

2.3. Preparation of catalysts

Typically, the as-prepared Co_xMn_y-L complex was mixed with five times weight of DCA by grinding in a mortar. The mixed powder was pyrolyzed in a tube furnace under argon atmosphere with the flow rate of 70 mL/min. The annealing temperature was programmed from room temperature to 550 ℃ with the rate of 5 ℃/min and kept at 550 ℃ for 2 h, then the temperature was increased to 900 ℃ with the rate of 2.5 ℃/min and kept at 900 ℃ for 3 h, then it was naturally cooled to room temperature. The as-obtained catalyst was grinded for activity test and characterization. For comparison, metal catalyst without N-doping (Co/Mn-C) and metal free catalyst (N@C) were also prepared.

2.4. Characterization of catalysts

Transmission electronic microscopy (TEM) and energy-dispersive X-ray analysis (EDX) were carried out on a FEI TF20 instrument. Powder X-ray diffraction (XRD) patterns were recorded on a Rigaku Ultima IV diffractometer. Metal content in samples were determined by inductively coupled plasma atomic emission spectroscopy (ICP-AES) on a Thermo ICAP6300 Radial. X-ray photoelectron spectroscopy (XPS) spectra were acquired on a ThermoFisher Scientific ESCALAB 250XI using monochromated Al Kalph source (150 W). CO_2 temperature-programmed desorption (CO_2-TPD) was conducted on a Quantachrome TPRWin v3.52. Before CO_2-TPD experiments, the catalysts were outgassed at 300 ℃ for 2 h in helium flow. Subsequently the catalysts were cooled down to 25 ℃ and adsorbed CO_2 for 1 h. The desorption of CO_2 was performed by heating from 50 ℃ to 800 ℃ at the rate of 20 ℃ min^{-1} in helium flow. H_2 temperature-programmed reduction (H_2-TPR) was performed on AutoChem II 2920 equipped with TCD detector. The sample was pretreated in argon flow (50 mL/min) at 200 ℃ for 1 h. After the sample cooled to 50 ℃, a mixture of 10% H_2 in Ar (50 mL/min) was introduced and the temperature was increased to 800 ℃ at a rate of 10 ℃/min. Raman spectra were acquired on a Renishaw inVia Micro-Raman Spectroscopy equipped with CCD detector at 633 nm. The mass spectrometry analysis for isotope labeled compounds was carried out on an ADC Bioscientific G6540B TOF-MS using electronegative mode.

2.5. Catalytic activity test of catalysts

In a typical reaction, 0.5 mmol HMF, 0.5 mmol Na_2CO_3, 50 mg catalyst, and 10 mL water were added into a 100 mL round-bottom flask. The flask was purged with O_2 for 6–8 times and the reactant mixture was stirred under 1 bar of O_2 at 85 ℃ for 10 h. The content of HMF and its derivatives in samples were analyzed by HPLC on Aminex® HPX-87H column (300 mm × 7.8 mm) using aqueous sulfuric acid (5 mM) as mobile phase at the flow rate of 0.6 mL/min.

2.6. Kinetic reaction of HMF oxidation at gram scale

Gram scale oxidation of HMF to FDCA was carried out in a 1000 mL three-neck flask with a water condenser. Specifically, 4 g Co-Mn/N@C, 40 mmol HMF, 40 mmol Na_2CO_3 and 400 mL H_2O were added into the flask in preheated oil bath. The reaction proceeded at 85 ℃ with O_2 bubbling (40 mL/min). During the course of reaction, samples were taken for HPLC analysis.

2.7. Isotopic labeling experiments

The isotopic labelling experiments were carried out in 8 mL vials. Specifically, 2 mg HMF, 2 mg Na_2CO_3, 5 mg catalyst, and 1 mL $H_2{}^{18}O$ ($H_2{}^{16}O$) were added into the vial, and the air in the vial was replaced by $^{16}O_2$ ($^{18}O_2$). The reaction proceeded at 50 ℃ for 6 h under 1 bar of molecular oxygen and the yield of FDCA achieved 96%. Then, the obtained products were analyzed by mass spectrometry.

3. Results and discussion

3.1. Screening of catalysts for HMF oxidation

For the development of catalysts, a range of Co and Mn-based metal-lignin complexes (Co_xMn_y-L) with different loading of Co and Mn have been prepared by metal-phenols coordination directed assembly. The prepared Co_xMn_y-L complexes were mixed with DCA and pyrolyzed at high temperature (600–1000 ℃) in inert atmosphere. Then, the resulting materials were used for HMF oxidation in aqueous phase using ambient pressure of O_2 as oxidant. As shown in Table 1, entries 1–2, the oxidation of HMF to FDCA cannot spontaneously proceed or in the presence of unpyrolyzed Co_4Mn_1-L complex. However, co-pyrolysis of Co_xMn_y-L complexes and DCA at 800 ℃ yield active materials with different reactivity toward HMF oxidation depending on the composition of metals in precursor (entries 3–8, Table 1). In comparison of the monometallic catalysts, N-doped carbon supported Co (entry 8 of Table 1) give a much higher yield of FDCA (89.1%) than Mn-based catalyst (entry 3 of Table 1, 9.7%). The results indicate that supported Co on N-doped carbon has a much better intrinsic activity for the selective oxidation of HMF than supported Mn. Additionally, the bimetallic catalyst derived from Co_4Mn_1-L (entry 7 of Table 1) exhibits the highest yield of FDCA (95.1%) surpassing monometallic catalysts and other bimetallic catalysts. For a better comparison, the turn over frequency (TOF) values as a function of molar ratio of Mn/Co in catalysts was demonstrated in Fig. S1. It indicates that the addition of Mn into the catalyst has a promotional effect on the reactivity of Co. The best catalytic system was Co_4Mn_1-L derived catalyst given the efficiency of total metals.

Furthermore, the influence of pyrolysis temperature on the catalytic performance of catalysts was investigated using Co_4Mn_1-L and DCA as precursors at 600 ℃, 700 ℃, 800 ℃, 900 ℃ and 1000 ℃. It can be seen in Table 1, entries 9–13 that the catalyst obtained at 900 ℃ give the best catalytic performance (93.4% of yield, entry 12). The carbonization temperature-dependent reactivity of catalysts can be attributed to high temperature induced metal aggregation and metal-support interaction.

3.2. Structural properties of Co-Mn/N@C

To better understand the effect of pyrolysis temperature on the reactivity of Co_4Mn_1-L derived catalysts, the metal particle size dispersion (PSD) of representative catalysts obtained at 800, 900 and 1000 ℃ was investigated by TEM. The TEM analysis in Fig. 1a–f show the detailed structural information and PSD of Co-Mn/N@C-800, Co-Mn/N@C-900, and Co-Mn/N@C-1000, respectively. As expected, the metal NPs size growth increases with the increase of calcination temperature owing to Ostwald-ripening mechanism. The average particle size is 12.79, 13.51, and 29.13 nm for Co-Mn/N@C-800, Co-Mn/N@C-900, and Co-Mn/N@C-1000, respectively. In contrast to Co-Mn/N@C-900, the decrease of the activity of Co-Mn/N@C-1000 can be mainly explained by the dramatic aggregation of metal NPs. Notably, almost all the metal NPs in Co-Mn/N@C-1000 are encapsulated in carbon nanotubes (CNT) due to high temperature induced particle migration and growth of CNT (Fig. 1c). The growth of CNT can be attributed to the pyrolysis of DCA in the presence of metal catalyst [26,29]. Meanwhile, high resolution TEM (HR-TEM) analysis, EDX and XRD were performed to provide more information about the most active Co-Mn/N@C-900 catalyst. HR-TEM reveal that the observed NPs in the catalyst are metal Co and encapsulated by 7–9 layers of graphitic carbon (Figs. 1g–i and S2). Furthermore, Dark field-scanning transmission electron microscopy (DF-STEM) equipped with EDX analysis was employed to offer an insight into the element dispersion of Co, Mn, N, C and O in Co-Mn/N@C-900 (Figs. 1j–n and S3). As shown in Fig. 1j–n, the results further confirm that the visible NPs on the carbon carrier are metal Co. Additionally, Mn and N elements are homogenously dispersed on carbon matrix. In coincidence with the TEM results, only metal Co related diffraction peaks are observed in the XRD pattern of the catalyst in Fig. 1o. The contents of Co and Mn in Co-Mn/N@C-900 catalyst are determined to be 12.84 wt% and 1.34 wt%, respectively, by ICP-AES

Table 1
Screening of precursor and pyrolysis temperature of catalysts for selective oxidation of HMF to FDCA ***a*** **−** ***f***.

Entry	Precursor [c]	Pyrolysis tem. (℃) [d]	HMF conv. (%) [e]	FDCA yield (%) [e]	TOF (h^{-1}) [f]
1[a]	No catalyst	–	5.2	–	–
2 [a]	Co_4Mn_1-L	–	10.1	–	–
3 [a]	Mn_5-L, DCA	800	48.9	9.7	0.03
4 [a]	Co_1Mn_4- L, DCA	800	96.2	50.1	0.08
5 [a]	Co_2Mn_3- L, DCA	800	97.8	58.2	0.10
6 [a]	Co_3Mn_2- L, DCA	800	100	83.3	0.14
7 [a]	Co_4Mn_1- L, DCA	800	100	95.1	0.17
8 [a]	Co_5- L, DCA	800	100	89.1	0.12
9 [b]	Co_4Mn_1- L, DCA	600	61.1	2.0	< 0.01
10 [b]	Co_4Mn_1- L, DCA	700	98.6	53.1	0.26
11 [b]	Co_4Mn_1- L, DCA	800	100	61.8	0.27
12 [b]	Co_4Mn_1- L, DCA	900	100	93.4	0.39
13 [b]	Co_4Mn_1- L, DCA	1000	92.2	31.1	0.12

[a] Reaction conditions: 0.2 mmol HMF, 1 equiv. Na_2CO_3, 50 mg catalyst, 10 mL H_2O, 85 ℃, 1 bar O_2, 10 h.
[b] Same as 'a' with 0.5 mmol HMF.
[c] bottom-right digits represent the addition (mmol) of Co and Mn per gram of lignin for complexes synthesis.
[d] Annealing treatment was conducted in argon flow for 3 h.
[e] The conversion and yield were determined by HPLC.
[f] TOF was calculated on the obtained FDCA with respect to the total amount of Co and Mn in catalysts.

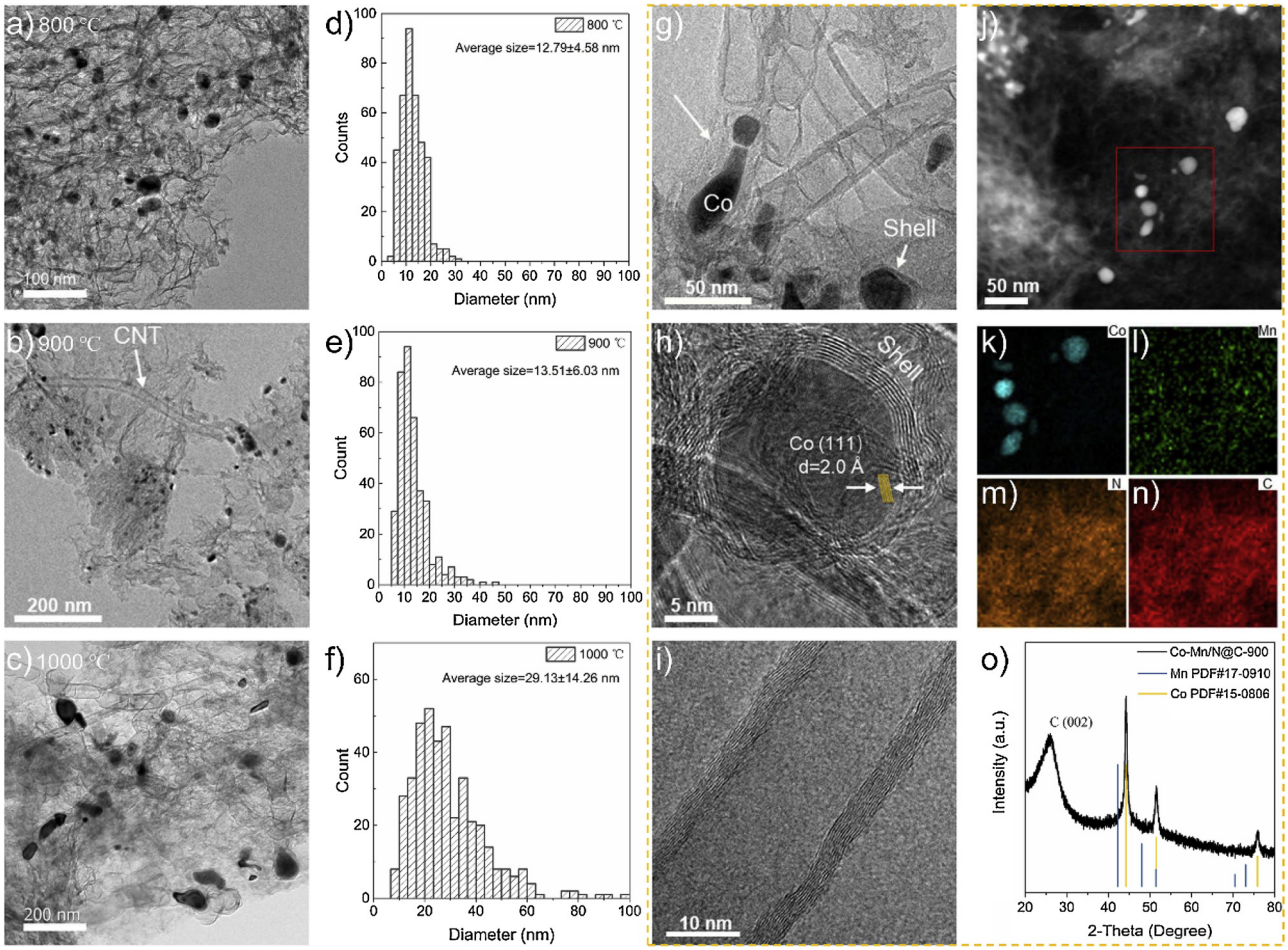

Fig. 1. Structural characterization of Co_4Mn_1-L derived catalysts at 800, 900, and 1000 ℃. (a–c) TEM images and (d–e) corresponding metal PSD of catalysts; (g–o) HR-TEM images, elemental mapping and XRD spectrum of Co-Mn/N@C-900.

(Table S1, entry 11). We speculate that the low content of Mn and strong coordination with N dopants depress the aggregation of Mn atoms, leading to atomically dispersion of Mn on N-doped carbon. However, the enhancement in the activity of Co-Mn/N@C-900 in comparision to Co-Mn/N@C-800 cannot explained by metal dispersion.

In addition to size effect, the electronic interaction between metal and support is critical for activating the reactivity of metal NPs [23]. Therefore, XPS was carried out to investigated the composition of carrier and electronic interaction between metal and support in Co-Mn/N@C-800, Co-Mn/N@C-900, and Co-Mn/N@C-1000. It can be seen in Fig. 2a, the O- and N-species in samples are decomposed with the increase of pyrolysis temperature. High resolution N1s and Co 2p XPS spectra in Fig. 2b–c show that the binding energy of pyridinic N shifts to higher position (+0.4 eV), while that of Co $2p_{3/2}$ shifts to lower energy (-0.6 eV), with increasing pyrolysis temperature. Such a phenomenon probably owing to the temperature-dependent metal-support interaction. For instance, Co-Mn/N@C-800 has high content of N species (13.89 atomic%, Fig. 2a) and relatively high content of electron-withdrawing pyridinic N (Figs. 2b, S4), functioning as electron acceptor [18]. However, elevated carbonization temperature (1000 ℃) results in the decomposition of pyridinic N (Figs. 2b, S4) and aggregation of Co NPs, which lead to the shift of main peak and a noticeable peak of Co° located at 778.3 eV in the Co2p spectrum (Fig. 2c). Meanwhile, the main peak of Mn $2p_{3/2}$ located at 641.8 eV can be assigned to Mn-N_x moieties, which are non-sensitive to pyrolysis temperature (Fig. 2d). [35] The introduced N-sites on carbon act as “solid ligands”, which improve the dispersion of metal atoms [17,22]. For the Mn species the N-sites coordinated with Mn atoms to form homogenously dispersed Mn-N_x moieties. Li and co-workers recently demonstrated that the strong interactions between N-doped carbon and metal atoms can drive the conversion of nanocatalysts to stable single-atom catalysts [36]. This strong interaction may be responsible for the atomically dispersion of Mn on Co-Mn/N@C. The XPS studies indicate the electron transfer from Co NPs to tailored graphitic carbon, which could strengthen the metal-support interaction. As depicted in Fig. 2e, tailored carbon with a higher work function can accept electrons from Co NPs until their Fermi level reaches equilibrium [23,37]. In addition to metal size effect, calcination temperature has significant effect on regulating the work function of heteroatoms-doped carbon by turning the N content and species [23]. In this case, Co-Mn/N@C-900 has the optimum electronic structure for HMF oxidation. Additionally, the addition of DCA promotes the thermal reduction of carbon and metals during annealing process is evidenced by comparing the XPS spectra of Co-Mn/N@C-900 (Fig. 2a–d) and Co/Mn-C-900 (Fig. S5).

The influence of N-doping on the basicity of catalyst surface was investigated by CO_2-TPD. In the TPD spectrum of Co/Mn-C, the CO_2 desorption peak at 95 ℃ can be attributed to physical adsorption, whereas, the main desorption peaks of Co-Mn/N@C shift to 142 ℃ and 197 ℃ (Fig. 3). The results confirm that N-doping endows the carbon support with basic sites. It has been demonstrated that tuning the basicity of carbon surface deposited with Au NPs is an effective strategy for enhancing the oxidation of HMF to FDCA [14]. Notably, the oxidation of HMF over supported non-noble metal NPs is limited [2], despite the extensive investigation of their metallic oxides [38,39].

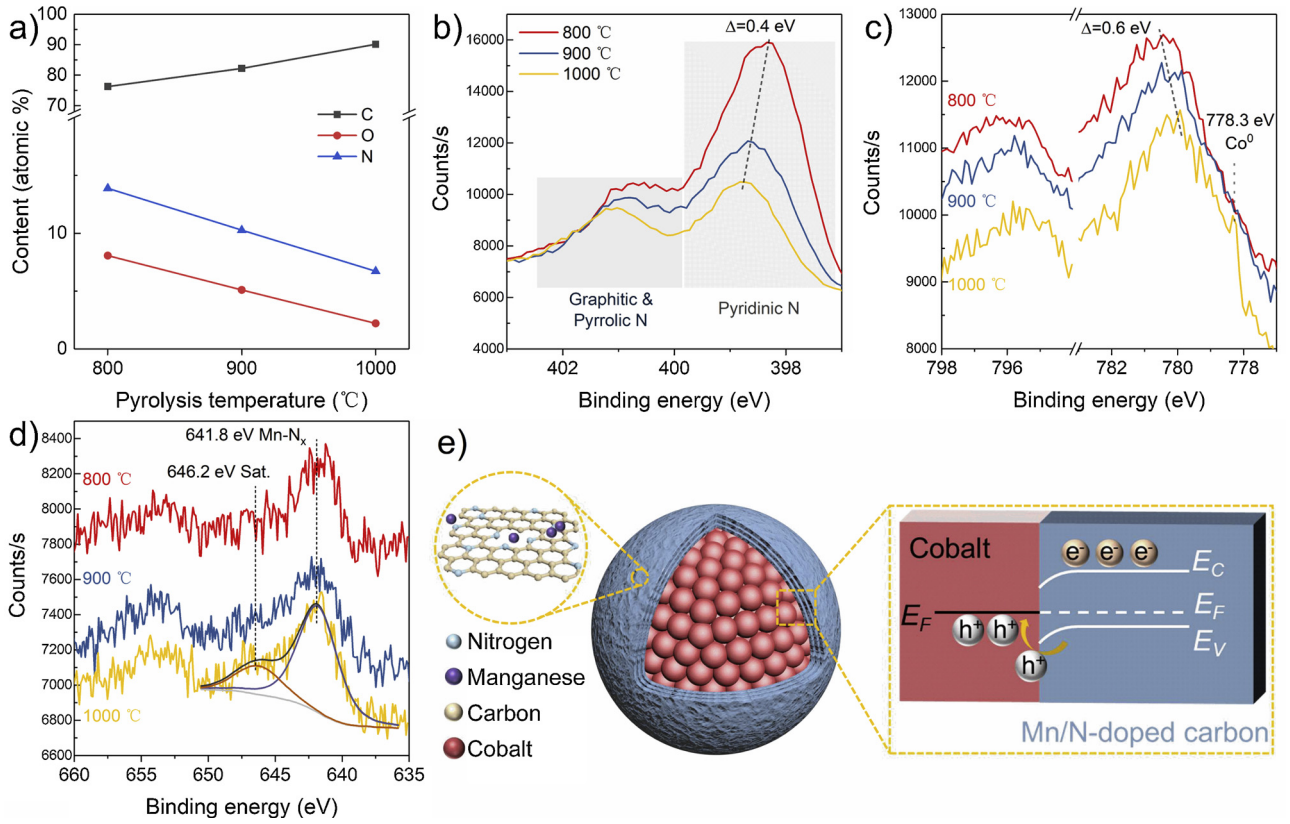

Fig. 2. Composition and metal-support interaction of Co_4Mn_1-L derived catalysts at 800, 900, and 1000 ℃ revealed by XPS. (a) the contents of C, O, and N in catalysts as a function of pyrolysis temperature; (b–d) high resolution N 1 s, Co 2p, and Mn 2p spectra of prepared catalysts at different temperature; (e) schematic demonstration of the electronic interaction in Co-Mn/N@C.

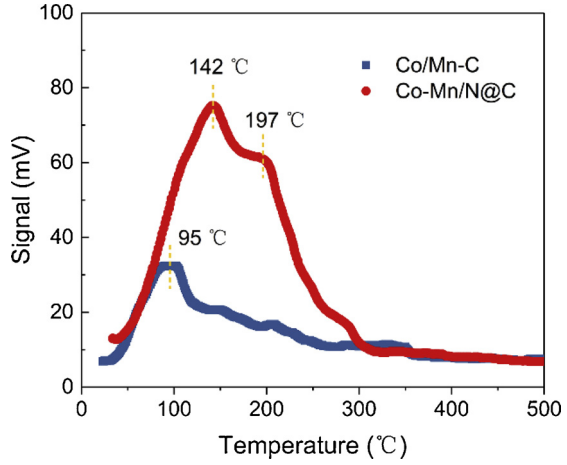

Fig. 3. CO_2-TPD for catalyst with and without N doping.

3.3. Effect of N-doping on the reactivity of Co-Mn/N@C for HMF oxidation

To understand the effect of N-doping, HMF oxidation were conducted over two control catalysts, Co/Mn-C and N@C. As shown in entries 1–2 in Table 2, conversion of HMF proceed in a non-selective type with negligible FDCA yield (1%) using Co/Mn-C or N@C as catalyst. In contrast, high yield of FDCA (96.1%) with excellent selectivity (96.4%) is achieved over Co-Mn/N@C (entry 3 of Table 2). The results reveal that N-doped graphitic carbon shells can activate inert Co NPs for selective oxidation of primary alcohols and aldehydes to carboxylic acids (i.e. FDCA) in aqueous system.

Furthermore, the influence of N-doping on the selective adsorption of substrate onto Co-Mn/N@C catalyst was investigated by kinetic

Table 2
Results of the oxidation of HMF under different conditions ***a*** **−** ***d***.

Entry	Catalyst	HMF conv. (%)[d]	Products yield (%)[d]			
			FDCA	HMFCA	FFCA	DFF
1[a]	Co/Mn-C	37.3	< 0.1	0.9	2.6	0.9
2[a]	N@C	39.5	0.1	1.7	0.6	–
3[a]	Co-Mn/N@C	99.7	96.1	1.7	0.6	–
4[b]	Co-Mn/N@C	18.0	0.5	1.7	3.1	–
5[c]	Co-Mn/N@C	62.5	0.1	2.8	0.1	–

[a] Reaction conditions: 0.5 mmol HMF, 1 equiv. Na_2CO_3, 50 mg catalyst, 10 mL H_2O, 85 ℃, 1 bar O_2, 12 h.
[b] Same conditions as 'a' without Na_2CO_3.
[c] Same conditions as 'a' and replaced O_2 with N_2.
[d] The conversion and yield were determined by HPLC.

reaction at gram scale. As shown in Fig. 4, HMF is rapidly consumed within the initial 2 h and completely transformed after 7 h. Finally, the desired FDCA and carbon balance reach the high products yield of 98.8% and 99%, respectively. Notably, HMFCA and FFCA are the only two detected intermediates during the reaction process, while DFF is not detected (Fig. S6). Therefore, the reasonable reaction pathway of HMF oxidation over Co-Mn/N@C follows route 1 (HMF→HMFCA→ FFCA→ FDCA) as depicted in Scheme 1. The reaction pathway for FDCA production over Co-Mn/N@C coincides with the supported Au and Pd catalysts [14,15,40] but totally different from the reported non-noble metal oxides (i.e. MnO_x-CeO_2, Fe_3O_4-CoO_x) [38,41] and Ru/C [42], which follows route 2 (HMF→DFF→FFCA→ FDCA) in Scheme 1. The distinct reaction pathway can be attributed to the preferential adsorption of −CHO side chain on HMF by the basic and positive surface of Co-Mn/N@C [14]. Therefore, N-doping impede the desorption of HMF derived products from catalyst surface. For instance,

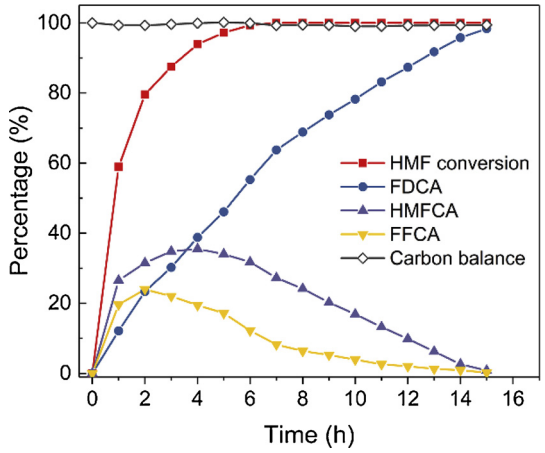

Fig. 4. Dynamic reaction for aerobic oxidation of HMF to FDCA over Co-Mn/N@C. Reaction conditions: 40 mmol HMF, 1 equiv. Na_2CO_3, 4 g Co-Mn/N@C, 400 mL H_2O, 85 ℃, O_2 bubbling 40 mL/min.

oxidation of HMF over Co-Mn/N@C under base free condition only give18% of HMF conversion and 5.3% of oxidized products (entry 4 of Table 2). One possible reason is the fact that the formed carboxylic acids prefer to adsorb on the basic surface of Co-Mn/N@C because of electrostatic interaction, resulting in the deactivation of catalytic centers [14]. Another important reason is that hydroxide ions is required for the activation of alcohol group over supported metal catalysts in aqueous phase [43].

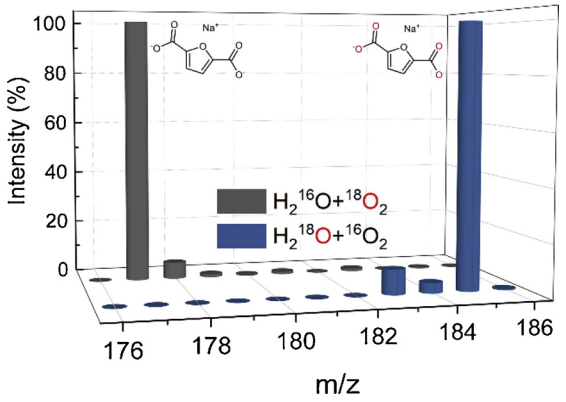

Fig. 6. Mass spectra of FDCA from HMF oxidation in ^{18}O labeled reagents.

3.4. Effect of Mn-doping on the reactivity of Co-Mn/N@C

To explore the promotion effect of highly dispersed Mn atoms in Co-Mn/N@C for HMF oxidation, the structure of a comparative catalyst derived from Co_5-L at 900 ℃ (Co/N@C) was investigated by TEM, XPS, H_2-TPR, and Raman spectroscopy. The average size of Co NPs is 14.86 nm determined by TEM (Fig. S8), which is larger than that of Co-Mn/N@C (13.51 nm). It indicates that the addition of Mn improves the dispersion of Co in Co-Mn/N@C by turning the composition of metals in catalyst (Table S1, entry 7, 11). Additionally, elemental analyses by XPS (Fig. 5a) reveal that more heteroatoms (i.e. N and O) are incorporated into Co-Mn/N@C catalyst, which may result in the increase of defects. High resolution N1 s XPS spectra further reveals that addition of Mn leads to higher concentration of pyridinic N (Fig. 5b). This phenomenon — addition of Mn leads to higher concentration of pyridinic N and total

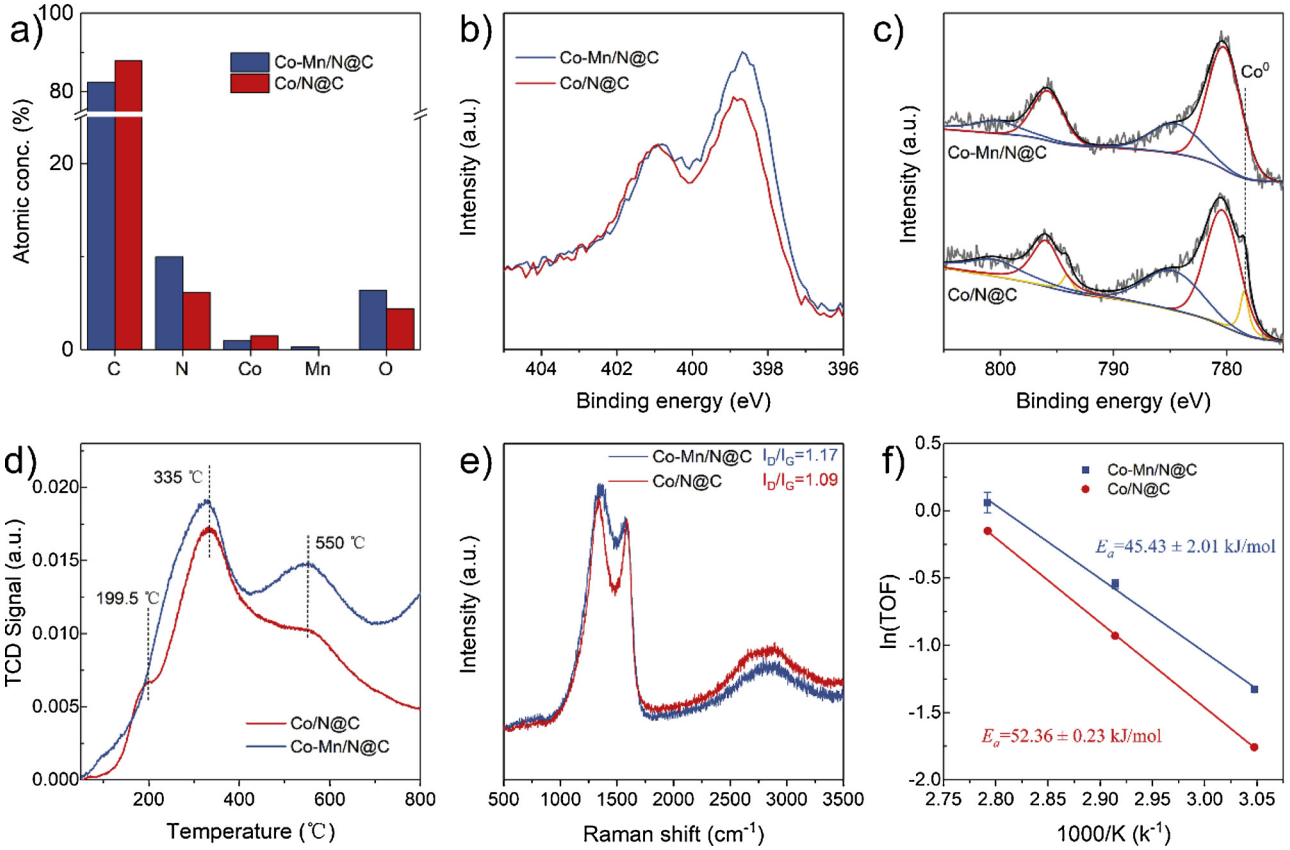

Fig. 5. Mn-doping on the structure and catalytic performance of catalyst. (a) elemental composition, (b) N1 s XPS spectra, (c) Co2p XPS spectra, (d) H_2-TPR profiles, (e) Raman spectra, and (f) Arrhenius plots for Co-Mn/N@C and Co/N@C. The TOF values were calculated based on the total amount of metals in catalyst.

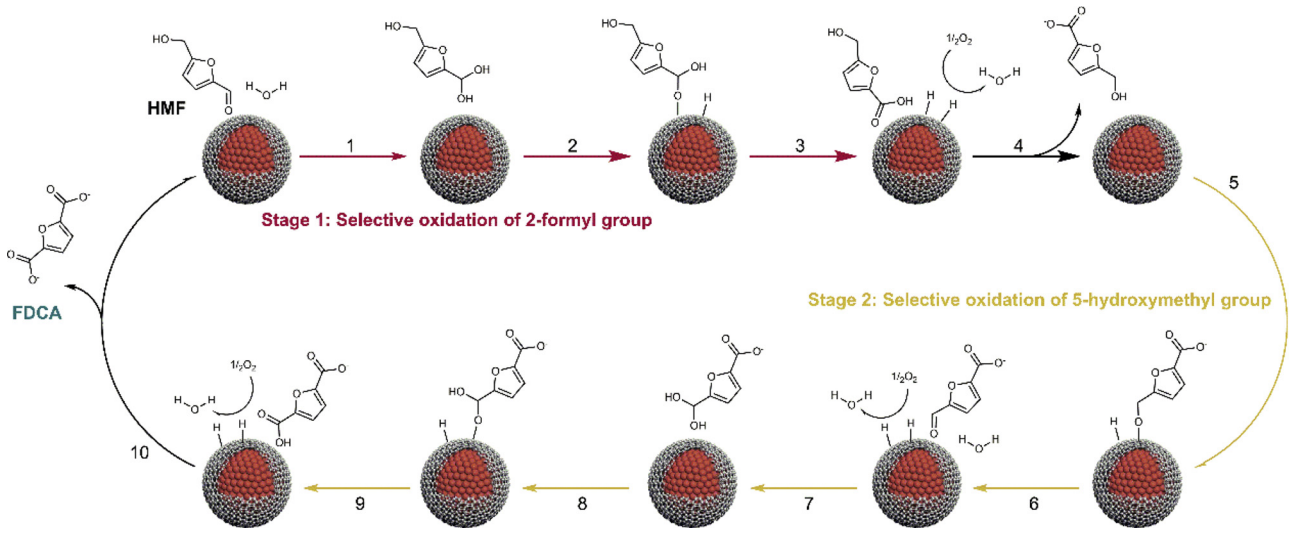

Fig. 7. Proposed reaction mechanism for selective oxidation of HMF to FDCA over Co-Mn/N@C.

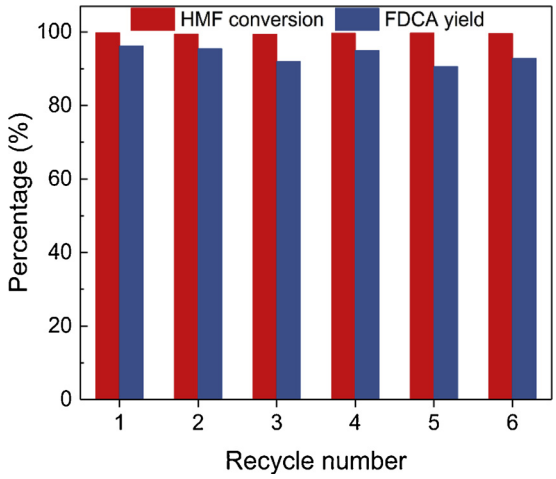

Fig. 8. Recycling experiments of Co-Mn/N@C. Reaction conditions: 0.5 mmol HMF, 1 equiv. Na_2CO_3, 80 mg catalyst, 10 mL H_2O, 85 ℃, 1 bar O_2, 12 h.

N — is well coincide with the work recently published by Liu et al. [44] Meanwhile, cationic Co (780.5 eV) and Co° (778.3 eV) are observed in the high-resolution Co2p XPS spectrum of Co/N@C, while only cationic Co in that of Co-Mn/N@C (Fig. 5c). The enhanced interfacial charge transfer between Co NPs and tailored carbon in Co-Mn/N@C can be attributed to the increase of total N and pyridinic N induced by Mn. The metal-support interaction was further studied by H_2-TPR. It can be seen in Fig. 5d, three reduction peaks at 199.5, 335, and 550 ℃ are observed in the TPR profile of Co/N@C. However, only two broader and stronger reduction peaks at 335, and 550 ℃ are found in the TPR profile of Co-Mn/N@C. The increased H_2 consumption at higher temperature can be attributed to the reduction of the Co species of strong interaction with Mn and N co-doped carbon [45]. Moreover, Raman spectra reveal that Mn-doping can slightly increases the defects of carbon (Fig. 5e), which is in agreement with XPS analysis (Fig. 5a). The above results demonstrate that the incorporation of Mn atoms in N-doped carbon can turn the electronic structure of Co-Mn/N@C, which results in the enhancement of reactivity. As shown in Fig. 5f, the E_a decreased from 52.36 kJ/mol to 45.43 kJ/mol with the presence of atomically dispersed Mn in catalyst for HMF conversion. It indicates that the homogenously distributed Mn atoms on carbon boost the reactivity of supported Co NPs by reducing the energy for HMF activation. Recently, Xiao and co-worker reported that the single-site Sn on TiO_2 promoted the supported metal nanoparticles for nitroarene hydrogenation via the creation of oxygen vacancies on TiO_2 surface [46]. Notably, the introduction of atomically dispersed metal atoms into support as promoters is emerging as a novel strategy for boosting the catalytic performance of heterogenous catalysts. Tuning the composition of multi-metal-lignin complexes can be used as a facile strategy to incorporate atomically dispersed metals into carbon carrier.

3.5. The role of O_2 and H_2O in HMF oxidation over Co-Mn/N@C

It has been reported that O_2 is critical for aerobic oxidation of alcohols [43]. As shown in entry 5 of Table 2, 62.5% of HMF is transformed over Co-Mn/N@C, whereas only trace oxidized products (total in 3%) are obtained in nitrogen atmosphere. To date, the precise role of O_2 for the aerobic oxidation of alcohols is still under debate, despite a few studies about supported Au or Pt catalysts [12,43]. Therefore, isotopic labeling experiments were conducted to reveal the function of O_2 and H_2O in the oxidation of HMF to FDCA over Co-Mn/N@C in aqueous system. As shown in Fig. 6, incorporation of ^{18}O into FDCA is only observed when using labeled $H_2{}^{18}O$ as solvent for HMF oxidation. The mass-to-charge ratio (m/z) of labeled FDCA at 185 in the spectrum indicates that four ^{18}O are incorporated during oxidation of HMF. These results are in good agreement with previous reports involving glycerol, ethanol, and HMF oxidation over Au/TiO_2 and Pt/C catalysts [12,43]. The isotopic labeling experiments reveal that HMF is react with hydroxide ions, dissociated from water in alkali solution, to form geminal diol during the oxidation of HMF over Co-Mn/N@C. The incorporation of four ^{18}O into FDCA can be attributed to the rapid exchange of ^{18}OH– with diol intermediates [12,43]. Meanwhile, the O_2 is essential for selective oxidation of HMF to FDCA. The possible function of O_2 is act as an electron scavenger to form reactive oxygen species, which remove the protons from H-metal intermediates to recover the catalyst [12,23]. Importantly, our studies proved that why water was the best solution for the oxidation of HMF to FDCA in most literatures [47–49].

3.6. Proposed reaction mechanism for selective oxidation of HMF to FDCA over Co-Mn/N@C

Based on the above results and literatures precedent, a probable reaction mechanism for HMF oxidation over Co-Mn/N@C is proposed and depicted in Fig. 7. The whole oxidation process can be divided into two main stages. During the first stage, the basic surface of Co-Mn/N@C catalyst preferably attract aldehyde sidechain of HMF and hydroxide ions dissociated from water [14]. The aldehydes undergo a

reversible hydration reaction to form germinal diols facilitated by adsorbed hydroxide ions on the catalyst surface [12,14]. The geminal diol intermediates are followed by oxidative dehydrogenation to generate HMFCA and desorbed from the catalyst surface in the assistance of base (Fig. 7, steps 2–4). In the second stage, C—H bond in the alcohol side chain is activated over Co-Mn/N@C catalyst surface to form the aldehyde intermediates, FFCA, (Fig. 7, steps 5 and 6), followed by further oxidation similar to stage 1 (Fig. 7, steps 7–10) to give the desired FDCA. During the whole process, O_2 plays an indirect role to removal of protons from catalyst surface [23].

3.7. Recyclability of Co-Mn/N@C catalyst

The recyclability and stability are main advantages of heterogeneous catalysts compared to enzymes and organometallic catalysts. As shown in Fig. 8, after six times of use, the HMF conversion and FDCA yield are still 99.5% and 92.7%, respectively. Moreover, aggregation of Mn atoms and oxidation of metal Co are not observed from the XRD pattern of recycled Co-Mn/N@C catalyst (Fig. S9). These results indicate that Co-Mn/N@C catalyst is recyclable and stable for selective oxidation of HMF to FDCA under reaction conditions. The reasonable explanation is that the N-doped carbon shells and nanotubes protect Co NPs from leaching and deactivation [50].

4. Conclusions

In summary, we proposed a facile, sustainable route for synthesizing Mn/N co-doped carbon supported Co nanocatalysts from Co/Mn-lignin complexes, which exhibited excellent performance for aerobic oxidation of HMF to FDCA in water. It was found that N-doping not only activated the reactivity of inert Co NPs, but also tuned the reaction pathway for selective HMF oxidation. Moreover, the highly dispersed Mn atoms in the catalyst were identified to boost the activity of Co NPs by turning the electronic structure of catalyst. Isotopic labeling experiments revealed that H_2O acts as an oxygen source of FDCA, whereas O_2 is as an electron scavenger and remove protons for regeneration of the catalyst. The integrated conversion of HMF and lignin from lignocellulosic biomass was demonstrated to maximizing the value of renewable wastes.

Notes

The authors declare no competing financial interest and conflicts.

Acknowledgment

This study was financially funded by the National Natural Science Foundation of China (NSFC, 21476016; 21776009).

Appendix A. Supplementary data

Supplementary material related to this article can be found, in the online version, at doi:https://doi.org/10.1016/j.apcatb.2018.12.046.

References

[1] Z. Zhang, G.W. Huber, Catalytic oxidation of carbohydrates into organic acids and furan chemicals, Chem. Soc. Rev. 47 (2018) 1351–1390.
[2] Z.H. Zhang, K.J. Deng, Recent advances in the catalytic synthesis of 2,5-furandicarboxylic acid and its derivatives, ACS Catal. 5 (2015) 6529–6544.
[3] M. Jong Kang, H. Park, J. Jegal, S.Y. Hwang, Y.S. Kang, H. Gil Cha, Electrocatalysis of 5-hydroxymethylfurfural at cobalt based spinel catalysts with filamentous nanoarchitecture in alkaline media, Appl. Catal. B-Environ. 242 (2018) 85–91.
[4] J.J. Bozell, G.R. Petersen, Technology development for the production of biobased products from biorefinery carbohydrates-the US Department of Energy's "Top 10" revisited, Green Chem. 12 (2010) 539–554.
[5] S. Albonetti, A. Lolli, V. Morandi, A. Migliori, C. Lucarelli, F. Cavani, Conversion of 5-hydroxymethylfurfural to 2,5-furandicarboxylic acid over Au-based catalysts: optimization of active phase and metal–support interaction, Appl. Catal. B-Environ. 163 (2015) 520–530.
[6] S. Thiyagarajan, W. Vogelzang, R.J.I. Knoop, A.E. Frissen, J. van Haveren, D.S. van Es, Biobased furandicarboxylic acids (FDCAs): effects of isomeric substitution on polyester synthesis and properties, Green Chem. 16 (2014) 1957–1966.
[7] A. Gandini, T.M. Lacerda, A.J. Carvalho, E. Trovatti, Progress of polymers from renewable resources: furans, vegetable oils, and polysaccharides, Chem. Rev. 116 (2016) 1637–1669.
[8] A.C. Dreischarf, M. Lammert, N. Stock, H. Reinsch, Green synthesis of Zr-CAU-28: structure and properties of the first Zr-MOF based on 2,5-furandicarboxylic acid, Inorg. Chem. 56 (2017) 2270–2277.
[9] F.A. Kucherov, E.G. Gordeev, A.S. Kashin, V.P. Ananikov, Three-dimensional printing with biomass-derived PEF for carbon-neutral manufacturing, Angew. Chem. Int. Ed. 56 (2017) 15931–15935.
[10] X.W. Han, C.Q. Li, Y. Guo, X.H. Liu, Y.G. Zhang, Y.Q. Wang, N-doped carbon supported Pt catalyst for base-free oxidation of 5-hydroxymethylfurfural to 2,5-furandicarboxylic acid, Appl. Catal. A-Gen. 526 (2016) 1–8.
[11] F. Neatu, R.S. Marin, M. Florea, N. Petrea, O.D. Pavel, V.I. Parvulescu, Selective oxidation of 5-hydroxymethyl furfural over non-precious metal heterogeneous catalysts, Appl. Catal. B-Environ. 180 (2016) 751–757.
[12] S.E. Davis, B.N. Zope, R.J. Davis, On the mechanism of selective oxidation of 5-hydroxymethylfurfural to 2,5-furandicarboxylic acid over supported Pt and Au catalysts, Green Chem. 14 (2012) 143–147.
[13] H.G. Cha, K.S. Choi, Combined biomass valorization and hydrogen production in a photoelectrochemical cell, Nat. Chem. 7 (2015) 328–333.
[14] B. Donoeva, N. Masoud, P.E. de Jongh, Carbon support surface effects in the gold-catalyzed oxidation of 5-hydroxymethylfurfural, ACS Catal. 7 (2017) 4581–4591.
[15] D. Lei, K. Yu, M.R. Li, Y.L. Wang, Q. Wang, T. Liu, P.K. Liu, L.L. Lou, G.C. Wang, S.X. Liu, Facet effect of single-crystalline Pd nanocrystals for aerobic oxidation of 5-hydroxymethyl-2-furfural, ACS Catal. 7 (2017) 421–432.
[16] R. Fang, P. Tian, X. Yang, R. Luque, Y. Li, Encapsulation of ultrafine metal-oxide nanoparticles within mesopores for biomass-derived catalytic applications, Chem. Sci. 9 (2018) 1854–1859.
[17] L. He, F. Weniger, H. Neumann, M. Beller, Synthesis, characterization, and application of metal nanoparticles supported on nitrogen-doped carbon: catalysis beyond electrochemistry, Angew. Chem. Int. Ed. 55 (2016) 12582–12594.
[18] Y.L. Cao, S.J. Mao, M.M. Li, Y.Q. Chen, Y. Wang, Metal/porous carbon composites for heterogeneous catalysis: old catalysts with improved performance promoted by N-doping, ACS Catal. 7 (2017) 8090–8112.
[19] X.H. Li, M. Antonietti, Metal nanoparticles at mesoporous N-doped carbons and carbon nitrides: functional Mott-Schottky heterojunctions for catalysis, Chem. Soc. Rev. 42 (2013) 6593–6604.
[20] T. Varga, G. Ballai, L. Vásárhelyi, H. Haspel, Á. Kukovecz, Z. Kónya, Co_4N/nitrogen-doped graphene: a non-noble metal oxygen reduction electrocatalyst for alkaline fuel cells, Appl. Catal. B-Environ. 237 (2018) 826–834.
[21] Q. Wei, X. Yang, G. Zhang, D. Wang, L. Zuin, D. Banham, L. Yang, S. Ye, Y. Wang, M. Mohamedi, S. Sun, An active and robust Si-Fe/N/C catalyst derived from waste reed for oxygen reduction, Appl. Catal. B-Environ. 237 (2018) 85–93.
[22] R.V. Jagadeesh, H. Junge, M.M. Pohl, J. Radnik, A. Bruckner, M. Beller, Selective oxidation of alcohols to esters using heterogeneous Co_3O_4-N@C catalysts under mild conditions, J. Am. Chem. Soc. 135 (2013) 10776–10782.
[23] H. Su, K.X. Zhang, B. Zhang, H.H. Wang, Q.Y. Yu, X.H. Li, M. Antonietti, J.S. Chen, Activating cobalt nanoparticles via the Mott-Schottky effect in nitrogen-rich carbon shells for base-free aerobic oxidation of alcohols to esters, J. Am. Chem. Soc. 139 (2017) 811–818.
[24] R.V. Jagadeesh, K. Murugesan, A.S. Alshammari, H. Neumann, M.M. Pohl, J. Radnik, M. Beller, MOF-derived cobalt nanoparticles catalyze a general synthesis of amines, Science 358 (2017) 326–332.
[25] Z. Gao, C. Li, G. Fan, L. Yang, F. Li, Nitrogen-doped carbon-decorated copper catalyst for highly efficient transfer hydrogenolysis of 5-hydroxymethylfurfural to convertibly produce 2,5-dimethylfuran or 2,5-dimethyltetrahydrofuran, Appl. Catal. B-Environ. 226 (2018) 523–533.
[26] Y. Yao, C. Lian, G. Wu, Y. Hu, F. Wei, M. Yu, S. Wang, Synthesis of "sea urchin"-like carbon nanotubes/porous carbon superstructures derived from waste biomass for treatment of various contaminants, Appl. Catal. B-Environ. 219 (2017) 563–571.
[27] C. Wang, J. Kang, P. Liang, H. Zhang, H. Sun, M.O. Tadé, S. Wang, Ferric carbide nanocrystals encapsulated in nitrogen-doped carbon nanotubes as an outstanding environmental catalyst, Environ. Sci.-Nano 4 (2017) 170–179.
[28] R.Q. Fang, R. Luque, Y.W. Li, Efficient one-pot fructose to DFF conversion using sulfonated magnetically separable MOF-derived Fe_3O_4 (111) catalysts, Green Chem. 19 (2017) 647–655.
[29] Y. Wu, X. Qiu, F. Liang, Q. Zhang, A. Koo, Y. Dai, Y. Lei, X. Sun, A metal-organic framework-derived bifunctional catalyst for hybrid sodium-air batteries, Appl. Catal. B-Environ. 241 (2019) 407–414.
[30] Z. Li, H. He, H. Cao, S. Sun, W. Diao, D. Gao, P. Lu, S. Zhang, Z. Guo, M. Li, R. Liu, D. Ren, C. Liu, Y. Zhang, Z. Yang, J. Jiang, G. Zhang, Atomic Co/Ni dual sites and Co/Ni alloy nanoparticles in N-doped porous janus-like carbon frameworks for bifunctional oxygen electrocatalysis, Appl. Catal. B-Environ. 240 (2018) 112–121.
[31] R.V. Jagadeesh, T. Stemmler, A.E. Surkus, M. Bauer, M.M. Pohl, J. Radnik, K. Junge, H. Junge, A. Bruckner, M. Beller, Cobalt-based nanocatalysts for green oxidation and hydrogenation processes, Nat. Protoc. 10 (2015) 916–926.
[32] R.V. Jagadeesh, A.E. Surkus, H. Junge, M.M. Pohl, J. Radnik, J. Rabeah, H. Huan, V. Schunemann, A. Bruckner, M. Beller, Nanoscale Fe_2O_3-based catalysts for selective hydrogenation of nitroarenes to anilines, Science 342 (2013) 1073–1076.
[33] G.H. Wang, X. Deng, D. Gu, K. Chen, H. Tuysuz, B. Spliethoff, H.J. Bongard, C. Weidenthaler, W. Schmidt, F. Schuth, Co_3O_4 nanoparticles supported on

mesoporous carbon for selective transfer hydrogenation of α,β-unsaturated aldehydes, Angew. Chem. Int. Ed. 55 (2016) 11101–11105.
[34] Zhong-Li Wang, Dan Xu, Hai-Xia Zhong, Jun Wang, Fan-Lu Meng, X.-B. Zhang, Gelatin-derived sustainable carbon-based functional materials for energy conversion and storage with controllability of structure and component, Sci. Adv. (2015) e1400035.
[35] W. Ju, A. Bagger, G.P. Hao, A.S. Varela, I. Sinev, V. Bon, B. Roldan Cuenya, S. Kaskel, J. Rossmeisl, P. Strasser, Understanding activity and selectivity of metal-nitrogen-doped carbon catalysts for electrochemical reduction of CO_2, Nat. Commun. 8 (2017) 944.
[36] S. Wei, A. Li, J.C. Liu, Z. Li, W. Chen, Y. Gong, Q. Zhang, W.C. Cheong, Y. Wang, L. Zheng, H. Xiao, C. Chen, D. Wang, Q. Peng, L. Gu, X. Han, J. Li, Y. Li, Direct observation of noble metal nanoparticles transforming to thermally stable single atoms, Nat. Nanotechnol. 13 (2018) 856–861.
[37] H.R. Chen, K. Shen, Q. Mao, J.Y. Chen, Y.W. Li, Nanoreactor of MOF-derived yolk-shell Co@C-N: precisely controllable structure and enhanced catalytic activity, ACS Catal. 8 (2018) 1417–1426.
[38] X. Han, C. Li, X. Liu, Q. Xia, Y. Wang, Selective oxidation of 5-hydroxymethylfurfural to 2,5-furandicarboxylic acid over MnO_x–CeO_2 composite catalysts, Green Chem. 19 (2017) 996–1004.
[39] D.K. Mishra, H.J. Lee, J. Kim, H.S. Lee, J.K. Cho, Y.W. Suh, Y. Yi, J. Kim, $MnCo_2O_4$ spinel supported ruthenium catalyst for air-oxidation of HMF to FDCA under aqueous phase and base-free conditions, Green Chem. 19 (2017) 1619–1623.
[40] X. Wan, C. Zhou, J. Chen, W. Deng, Q. Zhang, Y. Yang, Y. Wang, Base-free aerobic oxidation of 5-hydroxymethyl-furfural to 2,5-furandicarboxylic acid in water catalyzed by functionalized carbon nanotube-supported Au–Pd alloy nanoparticles, ACS Catal. 4 (2014) 2175–2185.
[41] S. Wang, Z. Zhang, B. Liu, Catalytic conversion of fructose and 5-hydroxymethylfurfural into 2,5-furandicarboxylic acid over a recyclable $Fe3O_4$–CoO_x magnetite nanocatalyst, ACS Sustain. Chem. Eng. 3 (2015) 406–412.
[42] G. Yi, S.P. Teong, Y. Zhang, Base-free conversion of 5-hydroxymethylfurfural to 2,5-furandicarboxylic acid over a Ru/C catalyst, Green Chem. 18 (2016) 979–983.
[43] B.N. Zope, D.D. Hibbitts, M. Neurock, R.J. Davis, Reactivity of the gold/water interface during selective oxidation catalysis, Science 330 (2010) 74–78.
[44] K. Liu, Z. Qiao, S. Hwang, Z. Liu, H. Zhang, D. Su, H. Xu, G. Wu, G. Wang, Mn- and N- doped carbon as promising catalysts for oxygen reduction reaction: theoretical prediction and experimental validation, Appl. Catal. B-Environ. 243 (2019) 195–203.
[45] G. Zhang, Y. Sun, Y. Xu, R. Zhang, Catalytic performance of N-doped activated carbon supported cobalt catalyst for carbon dioxide reforming of methane to synthesis gas, J. Taiwan Inst. Chem. E. (20) (2018) 1–11, https://doi.org/10.1016/j.jtice.2018.1007.1016.
[46] L. Wang, E. Guan, J. Zhang, J. Yang, Y. Zhu, Y. Han, M. Yang, C. Cen, G. Fu, B.C. Gates, F.S. Xiao, Single-site catalyst promoters accelerate metal-catalyzed nitroarene hydrogenation, Nat. Commun. 9 (2018) 1362.
[47] X. Han, L. Geng, Y. Guo, R. Jia, X. Liu, Y. Zhang, Y. Wang, Base-free aerobic oxidation of 5-hydroxymethylfurfural to 2,5-furandicarboxylic acid over a Pt/C–O–Mg catalyst, Green Chem. 18 (2016) 1597–1604.
[48] B. Liu, Y. Ren, Z. Zhang, Aerobic oxidation of 5-hydroxymethylfurfural into 2,5-furandicarboxylic acid in water under mild conditions, Green Chem. 17 (2015) 1610–1617.
[49] Z. Zhang, J. Zhen, B. Liu, K. Lv, K. Deng, Selective aerobic oxidation of the biomass-derived precursor 5-hydroxymethylfurfural to 2,5-furandicarboxylic acid under mild conditions over a magnetic palladium nanocatalyst, Green Chem. 17 (2015) 1308–1317.
[50] J. Deng, D. Deng, X. Bao, Robust catalysis on 2D materials encapsulating metals: concept, application, and perspective, Adv. Mater. 29 (2017) 1606967.